



In situ measurement of deposit layer formation during skim milk filtration by MRI

Nicolas Schork¹  | Sebastian Schuhmann¹ | Hermann Nirschl¹ | Gisela Guthausen^{1,2} 

¹Karlsruhe Institute of Technology (KIT), Institute of Mechanical Process Engineering and Mechanics, Karlsruhe, Germany

²Karlsruhe Institute of Technology (KIT), Chair of Water Chemistry and Water Technology, Karlsruhe, Germany

Correspondence

Gisela Guthausen, Karlsruhe Institute of Technology (KIT), Institute of Mechanical Process Engineering and Mechanics, Karlsruhe 76131, Germany.
Email: gisela.guthausen@kit.edu

Funding information

This IGF Project of the FEI is supported via AiF within the program for promoting the Industrial Collective Research (IGF) of the German Ministry of Economic Affairs and Energy (BMWi), based on a resolution of the German Parliament.

Abstract

Filtration and separation via membranes are key processes in food processing. One major application of membrane filtration is in the dairy industry, aiming for the separation of different milk proteins. The various chemical components of milk possess different physiochemical properties and can be used most effectively in food processing if they are separately available and remain in their native state. Microfiltration of skim milk allows a fractionation of the milk proteins casein and whey by size. A deposit is formed on the membrane surface mainly but not exclusively by micellar casein proteins during filtration. Membrane pore blockage by whey proteins and fouling occur during membrane filtration, negatively affecting the yield of the whey protein fraction. Skim milk filtration and the deposit layer formation were measured time and spatially resolved by *in situ* magnetic resonance imaging (MRI). The nature of the fouling layer was investigated during dead-end filtration in ceramic hollow fiber membranes. MRI was used to further clarify the influence of operating conditions on separation and filtration mechanisms that are responsible for growth of the fouling layer and its reversibility. The MRI measurements were analyzed for a detailed description of skim milk filtration by modeling the signal intensity distribution.

KEYWORDS

¹H, casein, filtration, membrane, MRI, NMR, protein separation, skim milk, whey

1 | INTRODUCTION

The dairy industry accounts for a large share of the European food production.^[1] Many food products consist of milk or contain milk components.^[1,2] By fractionating milk into its components, a more reliable and reproducible composition of many dairy products can be achieved, allowing new products and different types of food coatings to be developed.^[3,4] Fat, casein, and whey proteins can be used more efficiently in the food production industry if available separately.^[5] The fractionation of skim milk also leads to a reduction of water content in the

product to be transported, which represents a considerable economic and ecological improvement.^[2]

Milk proteins are known for their ability to be functional ingredients because of their high nutritional value and specific functionality.^[6] Particularly concentrated casein solutions and powders are often used, for example, as an additional source of protein, standardization of dairy products, stabilizers for meat or confectionery, pharmaceuticals, and in paper and adhesives industry.^[2,7,8] There are many ways to produce caseins, e.g., by acid or alkaline precipitation or by microfiltration or ultrafiltration of skim milk with

the help of membranes, which is further regarded in this publication.^[1,2,6,7] During filtration, the casein protein micelles remain in their native state and do not undergo structural, that is, functional changes.^[6,9,10] Generally speaking, there are two main flow configurations of membrane filtration processes that can be differentiated. In cross-flow filtration mode, the feed flow is tangential to the membrane surface, whereas in dead-end filtration mode, the direction of the feed flow is normal to the membrane surface. In industrial processes, skim milk is most often filtered in cross-flow filtration mode to obtain highly concentrated micellar casein solutions.^[1,5,11–13] To gain insights into the properties, function, and structure of the deposit layer, a dead-end filtration mode was used due to a better compatibility with the needs of nuclear magnetic resonance imaging (MRI). During filtration, proteins and other ingredients of the skim milk form a deposit layer on the membrane.^[14] This layer consists of densely packed casein and whey proteins, resulting in an additional filtration resistance and a steep decline in permeate flux after a short period of time.^[2,10,15,16] Furthermore, the deposit layer retains smaller whey proteins by approx. 50%.^[17] As an object of current research, it was shown that not only whey but also casein proteins can penetrate the membrane, resulting in an insufficient protein separation and fractionation.^[18–20] By means of membrane filtration, a complete retention of micellar casein is hardly achieved, as is the complete permeation of whey proteins.^[16] Deposit layer formation in milk filtration has, so far, been investigated in off-line experiments^[13,15,21–23] and in *in situ* Small-angle X-Ray Scattering (SAXS) measurements using an X-ray transparent setup to measure filtration with a flat-sheet membrane.^[24,25] In order to obtain detailed insight into the phenomena and mechanisms of deposit layer in an opaque hollow fiber setup during the fractionation of micellar caseins, time-resolved and spatially resolved measurements are essential. MRI was used for an *in situ* analysis of many membrane processes.^[17,26–29] MRI allows not only a measurement in an optically transparent setup but is also a non-invasive analysis method in opaque ceramic hollow fibers that are used in this publication.^[17,30–34]

2 | EXPERIMENTAL

2.1 | Feed solutions

To ensure reproducible and reliable experimental conditions, a skim milk produced from soluble “skim milk powder low heat” from “Milk and Whey Ingredients”, Sachsenmilch Leppersdorf GmbH, Germany was used

TABLE 1 Composition of the skim milk powder used for the filtration experiments and selected properties

Skim milk content or property	Value
Water	3.44% _{w/w}
Fat	0.47% _{w/w}
Protein	33.98% _{w/w}
Lactose	53.87% _{w/w}
Ash	7.82% _{w/w}
pH	6.5
Temperature (<i>T</i>)	25 °C

(Table 1). For the experiments, the solution was prepared by dissolving $m_{\text{powder}} = 107.85$ g of powder in $V_{\text{water}} = 1$ L of demineralized water resulting in 2.8%_{w/w} of casein protein. The composition of the aqueous solution was orientated on the protein composition found in milk, hence, 2.8%_{w/w} casein (approx. 50–400 nm)^[14] and 0.6%_{w/w} whey proteins (approx. 2 nm), assuming a typical share of 80% of casein and 20% whey protein.^[1,7,35,36] The skim milk powder was stirred with a magnetic stirrer for at least 1 hr to ensure a complete rehydration and dissolution of the skim milk powder. pH of the rehydrated skim milk was between 6.5 and 7. All experiments were performed at room temperature of about $T = 25$ °C. In the following, the rehydrated skim milk powder is referred to as skim milk.

2.2 | Contrast agent nanomag-D-spio embedded in dextran and casein coating

In order to obtain a better MRI contrast between feed solution and protein deposit, a contrast agent was added to the skim milk feed solution prior to the filtration. The contrast agent “nanomag-D-spio” purchased from micromod Partikeltechnologie GmbH, Germany was prepared by precipitation of iron oxide (approx. 66%_{w/w} according to the distributor) embedded into a layer of dextran ($M_w = 40$ kDa) and has a mean particle diameter of 100 nm. An additional coating with casein proteins was added to guarantee chemical compatibility with the feed solution. For the filtration, the contrast agent is added to the feed to obtain an iron concentration of $c_{\text{Fe}} = 4.27 \cdot 10^{-6}$ mol_{Fe}/L.

2.3 | Hollow fiber membrane

For the fractionation of the proteins in skim milk, ceramic hollow fiber membranes were used as provided by MANN+HUMMEL GmbH, Ludwigsburg, Germany. The membranes were filtered in an in–out filtration

mode, in which the feed solution is filtered through the radially asymmetric structure of the porous Al_2O_3 ceramics. The inner coating of the membrane lumen with an inner diameter of 1.9 mm and outer diameter of 3.2 mm^[17,29,30] has an average pore diameter of 40 nm and determines the filtration characteristics. The highly porous layer on the outside of the active layer provides mechanical stability for the inner, selective layer without increasing the membrane resistance too much. The hollow fiber provides a good mechanical and thermal stability and allows aggressive chemical cleaning often needed for sanitary purposes in food processing. The pure water permeability was measured between $J_0 = 251 \text{ L}/(\text{m}^2 \text{ h bar})$ and $J_0 = 410 \text{ L}/(\text{m}^2 \text{ h bar})$ for used ceramic hollow fiber membranes.

2.4 | *In situ* filtration experiments

For the *in situ* filtration of skim milk, a single hollow fiber was placed into a filtration module that was mounted into the probe and then inserted into the tomograph (Figure 1a,b). The single fiber module was connected to the filtration periphery. With the help of the periphery, pressure measurements and a gravimetric determination of the permeate mass are possible and can be recorded as a function of time.

For *in situ* MRI filtration measurements, the filtration module was placed into a Bruker Avance HD III SWB 200 MHz spectrometer. A 20 mm birdcage of the MICWB40 series was used to move the module freely in the tomograph (Figure 1). The measurements were done in a segment of the module of about 20 mm below the permeate outlet (Figure 1b). Different feed pressures (0.5, 1.0, and 1.5 bar) were realized to explore the pressure dependence of the deposit formation. The experiments were performed in dead-end filtration mode. A complete description of the

filtration setup and its configuration options can be found in previous studies.^[32–34]

2.5 | MRI hardware and methods

In order to characterize the nanomag-D-spio contrast agent, dilution series of the particles were produced. The first dilution series in water was performed using demineralized water where each dilution step was carefully mixed to ensure a homogeneous dispersion of the particles. Even after weeks, no sedimentation or agglomeration of the nanoparticles was observed. In the second and third dilution series, the nanoparticles were added to skim milk. One of the solvents is skim milk with the same casein protein concentration that was used as feed in the MRI-filtration experiments (2.8%_{w/w}). The other solution was a higher concentrated skim milk that consisted of 2.5 times the casein protein concentration (7%_{w/w}) to model the situation of the deposit.

^1H inversion recovery (IR) and CPMG pulse sequences were applied at $\nu_L = 200 \text{ MHz}$ for T_1 and T_2 relaxation experiments, necessary to measure the relaxivities of these new contrast agents. The measurements were also performed in a MICWB40 birdcage with a standard 5 mm nuclear magnetic resonance (NMR) sample tube in the center of the birdcage. The important parameters for both pulse sequences are listed in Table 2. The IR timing list as well as the echo-counter list and the echo time in the CPMG experiments were adjusted for the different solutions.

The development of the deposit inside the membrane lumen was characterized by measuring MR images with a rapid acquisition with relaxation enhancement (RARE) as was done in the case of alginate filtration.^[17,30] An appropriately high repetition time T_R and a low rapid acquisition with relaxation enhancement factor (RF) reduce flow artefacts that prohibit a quantification. To

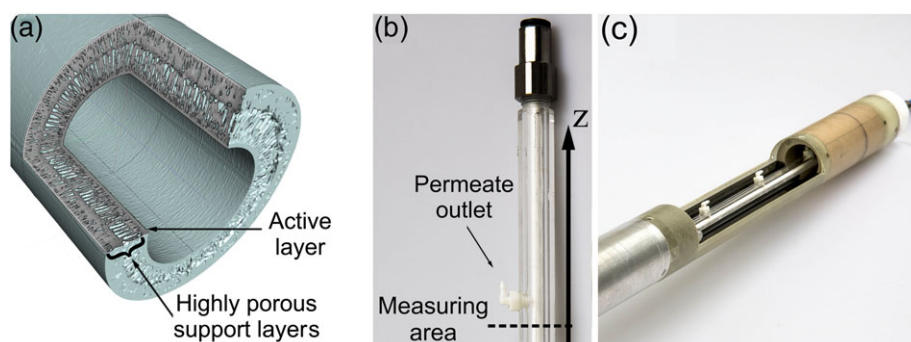


FIGURE 1 (a) A three-dimensional reconstruction of a μCT measurement of the ceramic hollow fiber membranes shows the thin active layer on the inside that is held in place by highly porous support layers. (b) The module for the single fiber filtration was made out of magnetic resonance imaging compatible materials and can be used with multiple outlets, where only one permeate outlet was used in the present experiments. (c) The filtration module was designed to fit into a 20 mm birdcage

TABLE 2 Typical inversion recovery and CPMG measurement parameters for the relaxation experiments

Pulse sequence parameter for IR and CPMG	Value
Repetition time T_R	8 s
Spectral band width (SWH)	4 kHz
Number of acquired data points	4096
Number of scans	4
Number of increments for relaxation observation	32

achieve an appropriate time resolution of the dynamic filtration process, an adequate measurement time while maintaining an appropriate image resolution was chosen. The measurement time was further reduced by partial Fourier imaging by sampling only 154 of 200 phase steps of the k -space resulting in a partial Fourier factor of 1.3 (Table 3). Multiple images were measured as a function of filtration time. The permeate flux of the dead-end filtration undergoes a steep decline in the first 20 min of the process as particles are deposited on the surface. After the initial decline, only a low permeate flux remains. The measurement time was selected so that a good temporal resolution of the filtration process was achieved, especially in its initial section that is of most interest.

2.6 | Quantification of the deposit layers

To quantify the signal intensity information of the deposit layer formation in the MR images, a radial averaging method was used. A mask of the inner membrane lumen was defined in a reference measurement by setting a

TABLE 3 Typical magnetic resonance imaging measurement parameters for the magnetic resonance images by rapid acquisition with relaxation enhancement

RARE MRI pulse sequence parameter	Value
T_R (T_1 weighting)	4 s
τ_E (T_2 weighting)	5.5 ms
$\tau_{E, \text{eff}}$ (T_2 weighting)	11 ms
Encoding order	Centric
Pixel size $\Delta x = \Delta y$	32.5 μm
RARE factor (RF)	2
Number of averages	1
Slice thickness	3 mm
Partial Fourier factor (phase)	1.3
Read steps	200
Phase steps	154
Scan time	5 min 8 s

signal threshold and deleting all measured voxels outside the membrane lumen that are below the set threshold. By applying this mask, the exact geometry of the membrane lumen can be extracted allowing also a quantification of geometries that are not perfectly cylindrical or even arbitrarily shaped. To quantify the signal intensities in the lumen, the geometry of the mask was continuously reduced pixel by pixel towards the center of the lumen. In a first iteration of the applied method, the mask was eroded with a disk-shaped object with a radius of two pixels. By continuously eroding the mask, an increasing deviation from the original geometry occurs. In this current version, the mask is therefore reduced with the image resize function (“imresize”) in MATLAB by two pixels in each direction. The bilinear interpolation of the image resize function results in a better replication of the original geometry in inner rings. In each of the defined rings, the signal intensity was averaged, maximizing the accuracy of the signal intensity information as well. A mean signal intensity was obtained as a function of radius for each image and therefore time step during filtration (Figure 2).

A radially symmetric and uniformly accumulated deposit layer was observed in the MRI images that made it possible to average the signal intensities over the entire circumference. The radial signal variation was explored in a next step to further characterize the deposit as a function of time and radius.

3 | RESULTS AND DISCUSSION

3.1 | Relaxation characterization of “nanomag-D-spio” coated with casein

To characterize the influence of the contrast agents on the water relaxation in pure water and skim milk, the relaxation rates R_1 and R_2 of the water peak in the NMR spectrum were measured. Because the filtration experiments were performed at a Larmor frequency of $\nu_L = 200$ MHz, and relaxation is known to be field dependent, the relaxation rates were measured at the same frequency using an IR and CPMG pulse sequence respectively (Figure 3). The magnetization buildups in IR experiments were satisfactorily described by a mono-exponential function revealing the longitudinal relaxation rate R_1 . The decay of the transverse magnetization was also modelled by a mono-exponential function that results in the transverse relaxation rate R_2 . When varying the contrast agent concentration in the solution, a linear dependence of the relaxation rates was observed. The slope of the fitted linear function results in the relaxivity r_1 and r_2 , respectively. A comparison of the obtained

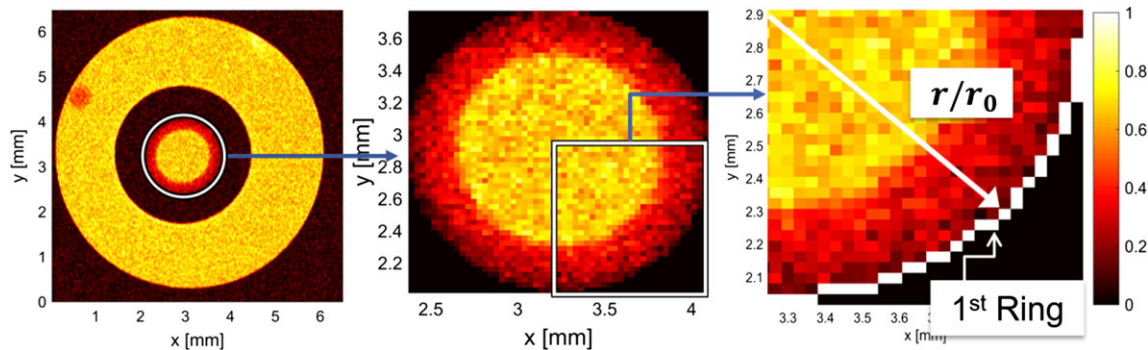


FIGURE 2 Determination of the signal intensity variation as a function of radius for each time step in the membrane lumen, exemplarily during a filtration with a feed pressure of $p = 1.5$ bar. A ring with a width of a single-pixel size in the form of the membrane's inner geometry is concentrically reduced with an image resize function pixel by pixel, keeping the form of the original membrane lumen. The mean signal intensity is calculated in each ring, allowing for a quantification of the deposit as a function of the reduced radius r/r_0 and filtration time t

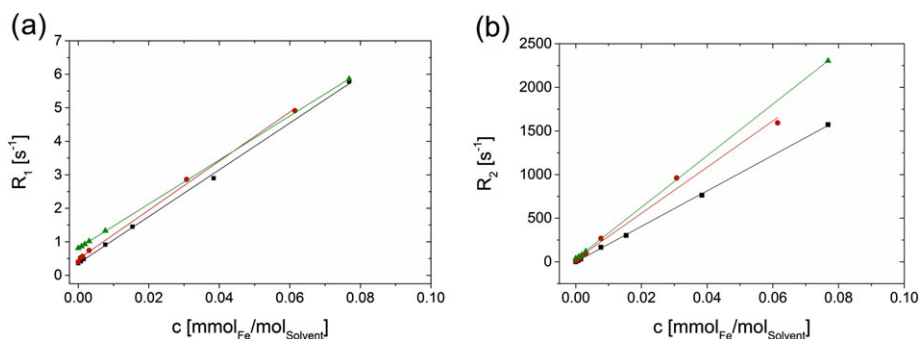


FIGURE 3 (a) Longitudinal and (b) transverse relaxation rates for different concentrations of the magnetic iron oxide nanocluster “nanomag-D-spio” with a functionalized casein coating measured at $\nu_L = 200$ MHz. The particulate contrast agent was diluted in demineralized water (black squares), a skim milk solution with the common 2.8%_{w/w} casein (red circles), and a higher concentrated skim milk with 7%_{w/w} casein (green triangles). A difference in the relaxivities was found for the different solvents, especially in the dominant r_2

results with different contrast agents from literature can be found in Table 4, in which the results are in the same order of magnitude as other iron oxide nanocrystallites.

The relaxivities in the dilution series with water are $r_1 = 69.8$ ($\text{mmol}_{\text{Fe}}/\text{mol}_{\text{Solvent}} \cdot \text{s}$)⁻¹ and $r_2 = 20373.1$ ($\text{mmol}_{\text{Fe}}/\text{mol}_{\text{Solvent}} \cdot \text{s}$)⁻¹. Water relaxivities were also measured in skim milk and in a skim milk solution with a higher concentration. In all cases, the amount

of water in the solution was used to calculate the iron to solvent ratio. The effect of a faster relaxation can mainly be seen in the transverse relaxation rates. In the higher concentrated and therefore more viscous solution the water relaxation rate increases. To better classify the relaxivity values, the relaxivities of the commonly used Gd-DTPA and other magnetic iron oxide nanocrystallites are listed in Table 4.

TABLE 4 Typical longitudinal and transverse relaxivities of different contrast agents caused by paramagnetic relaxation enhancement

Contrast agent	Solvent	d_p	Coating	r_1	r_2
Nanomag-D-spio	Water	100 nm	Casein	69.8 ($\text{mmol}_{\text{Fe}}/\text{mol}_{\text{Solv.}} \cdot \text{s}$) ⁻¹	20373.1 ($\text{mmol}_{\text{Fe}}/\text{mol}_{\text{Solv.}} \cdot \text{s}$) ⁻¹
Nanomag-D-spio	Skim milk	100 nm	Casein	76.2 ($\text{mmol}_{\text{Fe}}/\text{mol}_{\text{Solv.}} \cdot \text{s}$) ⁻¹	26479.9 ($\text{mmol}_{\text{Fe}}/\text{mol}_{\text{Solv.}} \cdot \text{s}$) ⁻¹
Nanomag-D-spio	2.5 x skim milk	100 nm	Casein	65.7 ($\text{mmol}_{\text{Fe}}/\text{mol}_{\text{Solv.}} \cdot \text{s}$) ⁻¹	29567.3 ($\text{mmol}_{\text{Fe}}/\text{mol}_{\text{Solv.}} \cdot \text{s}$) ⁻¹
MagAlg ^[30,37]	Water	100 nm	Alginate	1.7 $\text{mM}^{-1} \text{s}^{-1}$	338.5 $\text{mM}^{-1} \text{s}^{-1}$
Gd-DTPA ^[38-40]	Water	-	DTPA	3.2 $\text{mM}^{-1} \text{s}^{-1}$ (37 °C)	4.0 $\text{mM}^{-1} \text{s}^{-1}$ (37 °C)

3.2 | Quantification of the deposit formation and impact of the filtration mechanisms as measured by MRI

It is possible to detect the progress of deposits on the inner surface of the optically opaque hollow fiber membrane by MRI. The deposit of milk proteins as well as residual fats can be observed as a function of filtration time. The amount of deposit towards the membrane surface increases as the dead-end filtration progresses during the in-out filtration in the hollow fiber. The fouling layer can be natively identified by low signal intensities that is further enhanced by the added contrast agents. As a comparison, the signal intensity ratio of the signal intensity at the membrane surface and the feed intensity $I_{\text{deposit}}/I_{\text{Feed}}$ was measured in a native contrast setting and with the added contrast agent, resulting in $I_{\text{deposit}}/I_{\text{Feed}} = 0.41$ and in $I_{\text{deposit}}/I_{\text{Feed}} = 0.24$, respectively. The enhancement of the contrast is given by the relaxivities (Figure 3). The contrast agents induce a dominantly negative T_2 -contrast as described above (Table 4). Due to the large r_2 , the signal intensity decreases with the concentration of relaxation agent.

The filtration was performed at a feed pressure of 1.5 bar *in situ* with the described feed composition and contrast agent concentration. Several MR images were acquired with the described settings (Table 3). A fast deposit formation of the active membrane area was observed because a thick deposit layer is visible after only a few minutes (Figure 4). At the end of the in-out filtration, the deposit layer covers almost 50% of the area of the membrane lumen. As a result of the accumulation, the permeate flux is largely reduced caused by an increasing filtration resistance. Additionally, a small air bubble with a lower signal intensity increases with filtration time in the top left corner of the filtration module (Figure 4).

After normalizing the image's intensity to the average feed signal intensity in the center of the lumen, a radial average of the signal intensity was calculated to further quantify deposit formation during filtration. As a result, the signal intensities were calculated as a function of filtration time t and radial distance from the active membrane layer r/r_0 (Figure 4d). The deposit of mainly casein and whey proteins as well as the contrast agent particles induce a negative image contrast. The mean

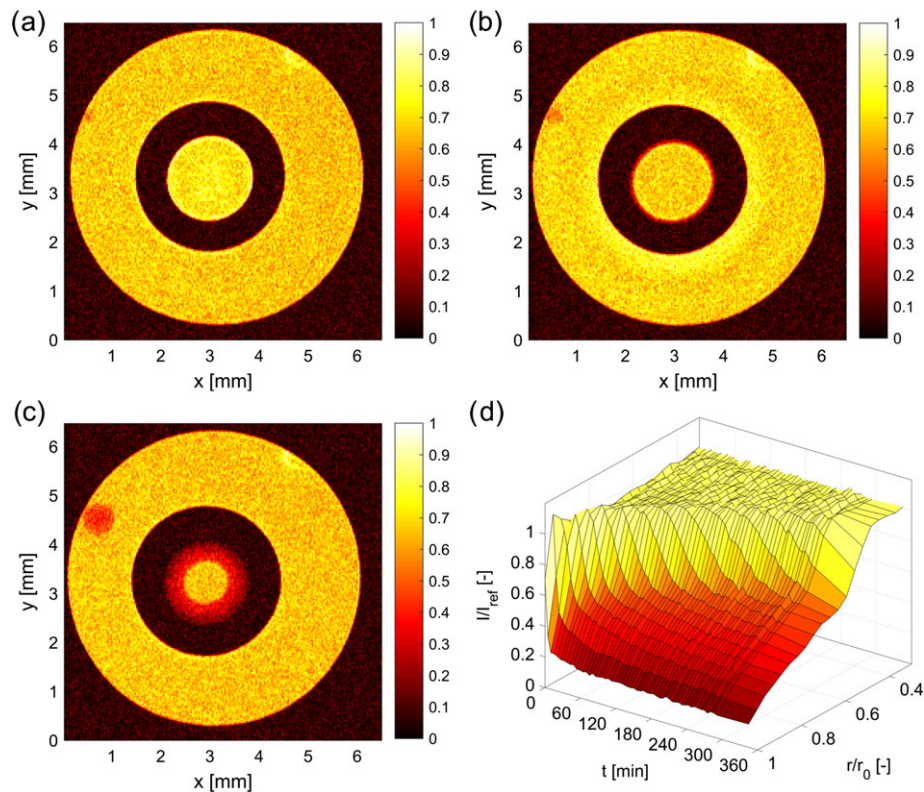


FIGURE 4 Axial images during an *in situ* dead-end filtration of skim milk with a feed pressure of 1.5 bar. (a) Magnetic resonance images of the filtration module with a centric hollow fiber before the filtration started. (b) After $t = 16$ min, the deposit can be seen that progressively accumulated on the active layer in the feed channel of the hollow fiber, (c) after a filtration time of $t = 5$ hr 45 min with an increased air bubble in the top left corner. (d) Normalized signal intensities as a function of filtration time and the reduced radius r/r_0 allow a quantification of the filtration (see Figure 2)

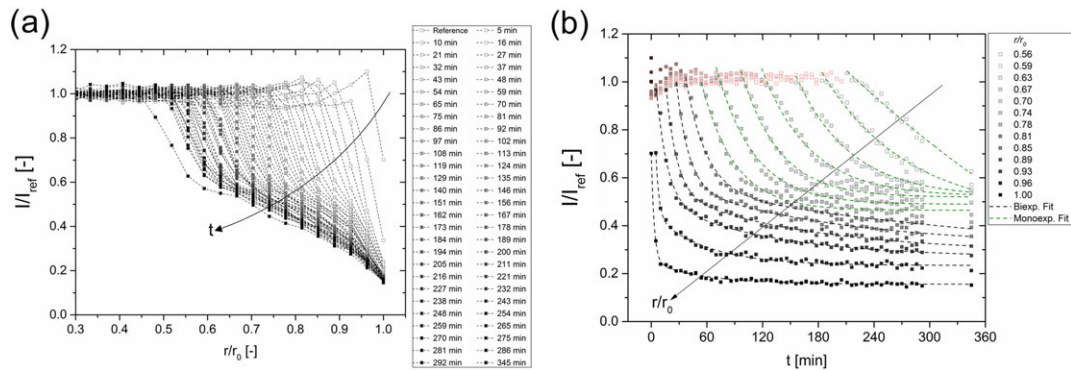


FIGURE 5 (a) Normalized mean signal intensities as a function of the reduced radius r/r_0 for each time step of filtration. (b) The signal intensities can also be regarded as a function of filtration time for each individual ring, that is, radius. For $r/r_0 = 0.81\text{--}1.00$, the signal intensities are described with a bi-exponential function (black dashed line) and for $r/r_0 \leq 0.78$, a mono-exponential function (green dashed line) is sufficient

signal intensities in the three-dimensional plot (Figure 4 d) can be viewed from both directions as either a function of reduced radius (Figure 5a) or as a function of filtration time (Figure 5b).

The first representation of the signal intensities as function of time (Figure 5, a) might seem more intuitive, as a decrease of the signal intensity can be observed close to the membrane at $r/r_0 = 1$.

In earlier publications, where a filtration with sodium alginate was performed, it was possible to describe the signal intensity with a mono-exponential function.^[34] The filtration mechanisms of sodium alginate with and without bivalent Ca^{2+} ions were quantified and described comprehensively with a time constant because it is well-known that bivalent ions change the molecular arrangement of the sodium alginate chains and thus the filtration mechanism. Concentration polarization and gel layer formation could be distinguished. These findings were in accordance with the classical filtration model. It describes the convective transport of the retained species to the membrane surface and back-diffusive transport in the opposite direction. Therefore, an accumulation of the retained substances results in a mono-exponential behavior.^[29]

In the present case, however, skim milk is a feed solution that is composed of a variety of different substances such as proteins, fats, lactose, and salts (Table 1) making it a rather complex filtration medium. The filtration and its mechanism are, therefore, not easily categorized into the classic schemes because it is not as clearly differentiated as in the case of sodium alginate, for example. A description of the filtration of soft and permeable colloids, as are the micellar casein proteins in skim milk, is subject of current research. A modelling approach was recently attempted.^[41,42] Because the experimental confirmation of the proposed filtration model is rather complex, a

different approach to quantify and compare the filtration at different pressures was chosen: The mean signal intensities are a function of filtration time, which can be modelled for each ring (Figure 5b).

In the first ring at the membrane surface ($r/r_0 = 1$), the signal intensity decreases right at the beginning of filtration as casein and whey proteins deposit on the membrane surface. Already after a few minutes, a sufficient amount of components of the skim milk accumulated in the first pixel ring, and the signal intensity starts to decrease in the subsequent rings for $r/r_0 < 1$.

The signal intensity angularly averaged in each ring could not be modelled by a mono-exponential function. This function did not describe the temporal behavior of intensities in the rings that are near the membrane surface ($r/r_0 = 0.81\text{--}1.00$). A bi-exponential function with two time constants $t_{c,1}$ and $t_{c,2}$ according to Equation (1) enabled a numerically sufficiently good description of the signal decay, whereas a simple mono-exponential decay adequately characterized the signal decay for the inner rings ($r/r_0 \leq 0.78$).

$$\frac{I}{I_{ref}} = A_1 \cdot \exp\left(-\frac{t}{t_{c,1}}\right) + A_2 \cdot \exp\left(-\frac{t}{t_{c,2}}\right) + y_0 \quad (1)$$

The fact that at least two time constants are necessary to describe the deposit formation during filtration is a strong indication that not only the proteins of the skim milk are accumulated but that also a consolidation or compaction of the deposited moieties takes place as the filtration time progresses. As a result, the filtration cannot be described as a pure concentration polarization of the proteins, that is, not only the skim milk components but also that the proteins might aggregate, and micelles might deform leading to a second form of deposit.^[43,44]

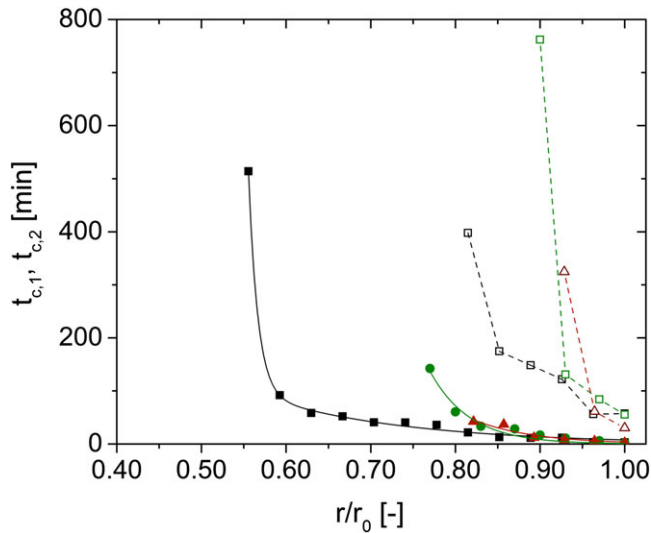


FIGURE 6 Time constants $t_{c,1}$ and $t_{c,2}$ of different feed pressures as a function of the reduced membrane lumen radius r/r_0 . The resulting time constants for $p = 1.5$ bar (filled black squares), $p = 1.0$ bar (filled green circles), and $p = 0.5$ bar (filled red triangles) can be plotted as a function of radius. The first time constant $t_{c,1}$ was modelled with Equation (2); full lines), whereas the second time constant $t_{c,2}$ is shown with a guide to the eye (dashed lines and open symbols)

TABLE 5 Resulting fit parameters of Equation (2)

Feed pressure	B [min]	r_{offset} [mm]	$h(p)$ [-]	$r(p) = h(p) * r_0$ [mm]
0.5 bar	25.6	0.86	0.071	66.92
1.0 bar	138.5	0.77	0.047	47.35
1.5 bar	122.05, 88.9	0.57	0.011, 0.176	10.10, 160.16

The two weighting factors in Equation (1) indicate that the first exponential function is dominant because A_1 is a factor five to 10 larger than A_2 .

The time constants were compared for the three different feed pressures (Figure 6). When applying higher

pressures in dead-end filtration, a larger amount of proteins accumulated, and a fast increase in deposit height was measured. As A_1 is dominant, the first time constant was further modelled by Equation (2):

$$t_{c,1} = B \cdot \exp\left(-\left(\frac{r - r_{\text{offset}}}{r_0}\right) \cdot \frac{1}{h(p)}\right). \quad (2)$$

The resulting fitting parameter (Table 5) show a dependence on the filtration parameters, e.g., feed pressure. The parameter r_{offset} is needed to model the data by Equation (2) adequately. Physically, it can be understood as a description of the maximal deposit height. In the case of $p = 1.5$ bar, a bi-exponential fit was applied.

Experiments were performed to measure the degree of reversibility in order to further investigate the nature of the deposit layer (i.e., structure and composition). Therefore, after a certain filtration time, the process was stopped by closing the feed valve and carefully releasing the filtration pressure to $p_{\text{Feed}} = 0$ bar by opening the retentate valve at the outlet of the hollow fiber, making sure that the deposit in the hollow fiber did not experience a large impulse and is not disrupted. Next, multiple MR images were measured in the time course (Figure 7).

Because there was no longer a feed pressure applied and the filtration was stopped, and the driving convective flow towards the active membrane layer in the hollow fiber vanished. Only back-diffusion of the deposits towards the inner membrane lumen was observed caused by the concentration gradient. A high degree of reversibility of the deposit layer that was built up during a dead-end filtration with $p_{\text{Feed}} = 0.5$ bar was observed: Almost the complete fouling layer is receding on a short-time scale. After about 30 min, the filtrated particles were already visibly diffusing back. Hardly any remaining gel-like deposit was measured that would be still attached to the active membrane layer (Figure 7c) indicating that the protein deposit is only

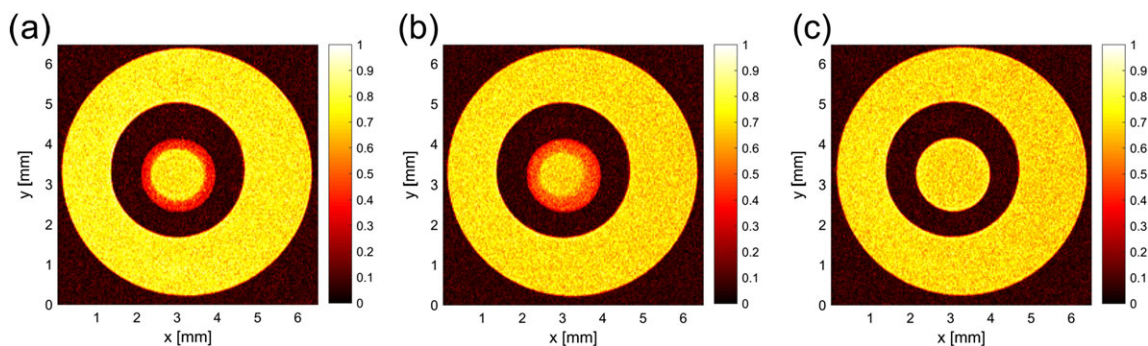


FIGURE 7 Reversibility of the deposit after a dead-end filtration with $p = 0.5$ bar. (a) At $t = 5$ min after pressure release, almost the entire deposit was found undisrupted near the active layer. (b) A loosening of the deposit layer was observed during the reversibility experiment, for example, at $t = 27$ min (c) At $t = 15$ hr almost the complete deposit layer disappeared, and a concentration equilibrium was detected. No deposit layer is visible on the length scale of the magnetic resonance imaging

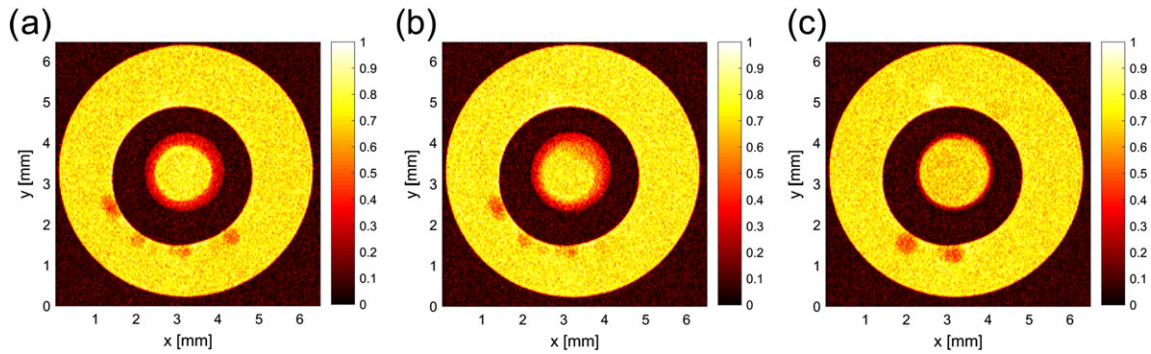


FIGURE 8 (a) After another filtration performed with $p = 1.0$ bar, the filtration was stopped, and the reversibility of the protein deposit layer was observed at $t = 5$ min. (b) A back-diffusion of the loose parts of the deposit was observed after a short period of time, for example, $t = 32$ min. (c) Even after a very long reversibility time of $t = 19$ hr, a deposit layer with a well-defined geometry is still visible on the inner surface of the hollow fiber. This indicates that parts of the deposit are more interlinked and not affected by back-diffusion

accumulated, and no aggregation or even gelation of the proteins had occurred at this feed pressure of $p = 0.5$ bar.

The nature and structure of the deposit layer that is built up during a dead-end skim milk filtration therefore depends on the applied feed pressure. During dead-end filtrations at higher pressures, a deposit layer develops, which is not reversed by back-diffusion (Figure 8). As a result, the filtration mechanism cannot be consistently described by a loose concentration polarization that can easily be reversed by back diffusion, when pressure is released, as has been shown in alginate filtration experiments in the work of Schuhmann et al.^[34] To further detach the remaining fouling layer and fully recover the filtration performance of the hollow fiber membrane, additional cleaning of the membrane layer must be performed. For example, back-washing or even chemical cleaning of the hollow fiber are needed to detach the adhesive or agglomerated part of the fouling layer.^[33]

4 | CONCLUSION

The longitudinal and transverse relaxation rates of magnetic iron oxide particles functionalized with casein proteins were measured for varying particle concentrations in demineralized water and two different skim milk concentrations. As often observed for superparamagnetic nanoparticles, the transverse relaxivity is dominant leading to a negative contrast in the MR images. When dissolving more skim milk powder in demineralized water, the viscosity of the solvent increases apart from the chemical composition. The longitudinal and transverse relaxivities depend on the solvent and its viscosity. Thus, the characterized magnetic iron oxide particles coated with casein proteins were utilized as a contrast agent for the MRI measurements to further increase the native image contrast.

In situ filtration MRI experiments with dissolved skim milk powder were performed at different feed pressures. The deposit in the ceramic hollow fiber membranes was observed as a function of filtration time in the dead-end mode. The fouling layer on the membrane was quantified as a function of the fiber radius by radially averaging the signal intensities within a given ring. A quantitative description of the signal intensity was achieved by modeling the signal intensity decays for radius r , discretized by the spatial resolution of MRI. The quantification showed not only an accumulation of substances on the membrane but also a consolidation or compaction of the accumulated proteins, evident especially at larger feed pressures. The deposit layer might be described by two regions that are a first thick and irreversible fouling layer and a second reversible concentration polarization layer. This interpretation of the nature of the deposit layer is consistent with reversibility experiments. The pressure-dependent reversibility in the pressureless experiment gave further insight into the nature of the deposit layer. The part of the deposit layer that is still attached to the membrane might indicate an aggregation of the accumulated proteins resulting in an insoluble layer whereas the concentration polarization was reversible caused by back-diffusion.

NOMENCLATURE

SYMBOLS AND ABBREVIATIONS

A_1	- fit parameter	[-]
A_2	- fit parameter	[-]
B	- fit parameter	[-]
c_{Fe}	- iron concentration	[mM _{Fe}]
I	- signal intensity	[a.u.]

(Continued)

I_{ref}	- normalized reference signal intensity	[a.u.]
J_0	- pure water permeability	[L/(m ² h bar)]
m	- mass	[g]
M_W	- molecular weight	[kDa]
SWH	- spectral width	[kHz]
p	- pressure	[bar]
R_1	- longitudinal relaxation rate	[s ⁻¹]
R_2	- transverse relaxation rate	[s ⁻¹]
r	- radial position	[mm]
r_{offset}	- fit parameter	[mm]
$r(p)$	- fit parameter	[mm]
r_0	- inner fiber radius	[mm]
r_1	- longitudinal relaxivity	[(mmol _{Fe} /mol _{Solvent} s) ⁻¹]
r_2	- transverse relaxivity	[(mmol _{Fe} /mol _{Solvent} s) ⁻¹]
RF	- RARE factor	[-]
T_1	- longitudinal relaxation time	[s]
T_2	- transverse relaxation time	[s]
T_R	- repetition time	[s]
T	- temperature	[°C]
t	- filtration time	[min]
$t_{c, 1/2}$	- time constant	[min]
V	- volume	[ml]
y_0	- fit offset	[-]

GREEK LETTERS

τ_E	- echo time	[ms]
$\tau_{E, effective}$	- effective echo time	[ms]
ν_L	- Larmor frequency	[MHz]

ACKNOWLEDGMENTS

Dr. U. Metzger provided the skim milk powder, which is highly appreciated. The authors thank the German Research Foundation (DFG) for financial support of the instrumental facility Pro²NMR. This IGF Project of the FEI is supported via AiF within the program for promoting the Industrial Collective Research (IGF) of the German

Ministry of Economic Affairs and Energy (BMWi), based on a resolution of the German Parliament.

ORCID

Nicolas Schork  <https://orcid.org/0000-0001-5891-8891>

Gisela Guthausen  <https://orcid.org/0000-0002-6444-2663>

REFERENCES

- [1] G. Brans, C. G. P. H. Schroën, R. G. M. van der Sman, R. M. Boom, *J. Membr. Sci.* **2004**, *243*, 263.
- [2] K.-V. Peinemann, S. Nunes, *Membrane Technology, Volume 4: Membranes for Water Treatment*, John Wiley & Sons, Weinheim **2010**.
- [3] S. Guilbert, N. Gontard, B. Cuq, *Packag. Technol. Sci.* **1995**, *8*, 339.
- [4] K. Khwaldia, C. Perez, S. Banon, S. Desobry, J. Hardy, *Crit. Rev. Food Sci. Nutr.* **2004**, *44*, 239.
- [5] Y. Pouliot, *Int. Dairy J.* **2008**, *18*, 735.
- [6] A. Hernández, F. M. Harte, *J. Dairy Sci.* **2009**, *92*, 5357.
- [7] P. Walstra, R. Jenness, *Dairy chemistry & physics*, John Wiley & Sons, Hoboken **1984**.
- [8] G. Daufin, J. P. Escudier, H. Carrere, S. Berot, L. Fillaudeau, M. Decloux, *Food Bioprod. Process.* **2001**, *79*, 89.
- [9] J. S. Mounsey, B. T. O'Kennedy, P. M. Kelly, *Lait* **2005**, *85*, 419.
- [10] H.-D. Belitz, W. Grosch, *Lehrbuch der Lebensmittelchemie*, Springer-Verlag, Berlin **2008**.
- [11] P. Punidadas, S. S. H. Rizvi, *Food Res. Int.* **1998**, *31*, 265.
- [12] T. Grein, W. Kuhn, A. Piry, U. Kulozik, S. Ripperger, *Filtrieren und Separieren* **2009**, *23*, 134.
- [13] A. Piry, W. Kuhn, T. Grein, A. Tolkach, S. Ripperger, U. Kulozik, *J. Membr. Sci.* **2008**, *325*, 887.
- [14] D. G. Dalgleish, M. Corredig, *Annu. Rev. Food Sci. Technol.* **2012**, *3*, 449.
- [15] A. Piry, A. Heino, W. Kuhn, T. Grein, S. Ripperger, U. Kulozik, *J. Dairy Sci.* **2012**, *95*, 1590.
- [16] A. D. Marshall, P. A. Munro, G. Tragardh, *Desalination* **1993**, *91*, 65.
- [17] F. Arndt, H.-J. Heidebrecht, N. Schork, S. Schuhmann, U. Kulozik, S. Schütz, H. Nirschl, G. Guthausen, in Proceedings of the XIII International Conference on the Applications of Magnetic Resonance in Food Science (Eds.: J. van Duynhoven, G. Guthausen), impublications, MR in Food 2016, **2016**, pp. 55.
- [18] J. Evans, J. Zulewska, M. Newbold, M. A. Drake, D. M. Barbano, *J. Dairy Sci.* **2010**, *93*, 1824.
- [19] N. D. Lawrence, S. E. Kentish, A. J. O'Connor, A. R. Barber, G. W. Stevens, *Sep. Purif. Technol.* **2008**, *60*, 237.
- [20] L. E. Coppola, M. S. Molitor, S. A. Rankin, J. A. Lucey, *Int. J. Dairy Technol.* **2014**, *67*, 467.
- [21] P. Qu, G. Gesan-Guiziu, A. Bouchoux, *J. Membr. Sci.* **2012**, *417*, 10.

- [22] W. Kühnl, A. Piry, U. Kulozik, *Chem. Ing. Tech.* **2008**, *80*, 1199.
- [23] B. J. James, Y. Jing, M. D. Chen, *J. Food Eng.* **2003**, *60*, 431.
- [24] Y. Jin, N. Hengl, S. Baup, F. Pignon, N. Gondrexon, M. Sztucki, G. Gesan-Guiziou, A. Magnin, M. Abyana, M. Karrouch, D. Bleses, *J. Membr. Sci.* **2014**, *470*, 205.
- [25] Y. Jin, N. Hengl, S. Baup, G. Maitrejean, F. Pignon, *J. Membr. Sci.* **2017**, *528*, 34.
- [26] P. Z. Culfaz, S. Bütehorn, L. Utü, M. Küppers, B. Blümich, T. Melin, M. Wessling, R. G. H. Lammertink, *Langmuir* **2011**, *27*, 1643.
- [27] S. Bütehorn, L. Utü, M. Küppers, B. Blümich, T. Wintgens, M. Wessling, T. Melin, *J. Membr. Sci.* **2011**, *371*, 52.
- [28] D. Airey, S. Yao, J. Wu, V. Chen, A. G. Fane, J. M. Pope, *J. Membr. Sci.* **1998**, *145*, 145.
- [29] S. Schuhmann, N. Schork, K. Beller, H. Nirschl, T. Oerther, G. Guthausen, *AIChE J.* **2018**, *64*, 4039.
- [30] F. Arndt, U. Roth, H. Nirschl, S. Schütz, G. Guthausen, *AIChE J.* **2016**, *62*, 2459.
- [31] F. Arndt, F. Ehlen, S. Schütz, H. Anlauf, H. Nirschl, *Sep. Purif. Technol.* **2016**, *171*, 289.
- [32] F. Arndt, S. Schuhmann, G. Guthausen, S. Schütz, H. Nirschl, *J. Membr. Sci.* **2017**, *524*, 691.
- [33] N. Schork, S. Schuhmann, F. Arndt, S. Schütz, G. Guthausen, H. Nirschl, *Microporous Mesoporous Mater.* **2018**, *269*, 60.
- [34] S. Schuhmann, N. Schork, K. Beller, T. Oerther, H. Nirschl, G. Guthausen, *AIChE J.* **2018**, *64*(11), 4093.
- [35] C. Kiesner, W. Hoffmann, P. Lorenzen, I. Clawin-Rädecker, D. Martin, H. Meisel, K. Einhoff, P. Hammer, P. Teufel, G. Suhren, *Standort Kiel* **2005**, *57*, 139.
- [36] R. Jenness, *Milk Proteins VI: Chemistry and Molecular Biology*, Academic Press, Cambridge **2012** 17.
- [37] G. Zoppellaro, A. Kolokithas-Ntoukas, K. Polakova, J. Tucek, R. Zboril, G. Loudos, E. Fragogeorgi, C. Diwoy, K. Tomankova, K. Avgoustakis, D. Kouzoudis, A. Bakandritsos, *Chem. Mater.* **2014**, *26*, 2062.
- [38] S. H. Koenig, R. D. Brown, *Prog. Nucl. Magn. Reson. Spectrosc.* **1990**, *22*, 487.
- [39] Y. Shen, F. L. Goerner, C. Snyder, J. N. Morelli, D. Hao, D. Hu, X. Li, V. M. Runge, *Invest. Radiol.* **2015**, *50*, 330.
- [40] M. Rohrer, H. Bauer, J. Mintorovitch, M. Requardt, H. J. Weinmann, *Invest. Radiol.* **2005**, *40*, 715.
- [41] A. Bouchoux, P. Qu, P. Bacchin, G. Gesan-Guiziou, *Langmuir* **2014**, *30*, 22.
- [42] W. R. Bowen, A. Mongruel, *Colloids Surf. A Physicochem. Eng. Asp.* **1998**, *138*, 161.
- [43] X. H. Li, J. X. Li, H. Wang, X. X. Huang, B. Q. He, Y. H. Yao, J. Wang, H. W. Zhang, H. H. Ngo, W. S. Guo, *AIChE J.* **2015**, *61*, 4377.
- [44] K. S. Y. Ng, M. Haribabu, D. J. E. Harvie, D. E. Dunstan, G. J. O. Martins, *J. Membr. Sci.* **2017**, *523*, 144.

How to cite this article: Schork N, Schuhmann S, Nirschl H, Guthausen G. *In situ* measurement of deposit layer formation during skim milk filtration by MRI. *Magn Reson Chem.* 2019;1–11. <https://doi.org/10.1002/mrc.4826>